academicJournals

Vol. 10(4), pp. 24-31, October 2017
DOI: 10.5897/AJMCSR2017.0712
Article Number: D53536766502
ISSN 2006-9731

http://www.academicjournals.org/AJMCSR

African Journal of Mathematics and Computer Science Research

Full Length Research Paper

Numerical solutions of the radiosity equation for a spherical quatrefoil on Mars

Yajni Warnapala* and Hien Ngo

Department of Mathematics, Roger Williams University, Bristol, Rhode Island 02809-2921, USA.

Received 19 July 2017; Accepted 21 September 2017

The Galerkin method is used to numerically solve the exterior boundary value problem for the radiosity equation for the spherical quatrefoil. The radiosity equation is a mathematical model for the brightness of a collection of one or more surfaces when their reflectivity and emissivity are given. On planet Mars the surface emissivity is closely related to its surface temperature. The radiosity of a surface is the rate at which the energy leaves that surface; it includes the energy emitted by a surface as well as the energy reflected from other surfaces.

Key words: Radiosity equation, Galerkin method, spherical quatrefoil.

INTRODUCTION

The mathematical model for the brightness of a collection of surfaces, when their reflectivity and emissivity are known in an exterior domain, is given by the Radiosity Equation:

$$u(P) - \frac{\rho(p)}{\pi} \int_S u(Q)G(P,Q)V(P,Q)dS_Q = E(P), P \in S \qquad (1)$$

Common methods such as the Direct Computation Method and the Modified Decomposition Method do not work as a method of solution as this is a nonlinear singular Fredholm Equation of the second order. Here, $u(P)$ is the radiosity or simply the brightness at P and emissivity is given by $E(P)$ and the reflectivity $\rho(P)$ is between zero and one. The assumption on the surfaces is that they are Lambertian diffuse reflectors. The method could also be extended to investigate alternative means of lighting on the planet such as, an artificial light source within a habitat since fluorescent lamps have also been reported to be the most appropriate light source for illumination on the interior of a spacecraft (Arvo, 1995). In addition, there have been published emissivity and reflectivity values for metal alloys and manufactured carbon-based fibers that could be used as inputs for a radiosity equation which will model a physical design for an interior space (deGroh et al., 2008). Simulations, considering material properties of internal components interacting with light waves inside the structure were used to generate data.

The spherical quatrefoil is controlled by one parameter. There are some numerical issues in this type of analysis; because of the singularity in the Kernel of the integral equation (Beyer, 1987). The Kernel G which is bounded when the surface is smooth is given by:

$$G(P,Q) = [\cos\beta_p \times \cos\beta_Q] / \mid (P-Q)^2 \mid$$

*Corresponding author. E-mail: ywarnapala@rwu.edu.

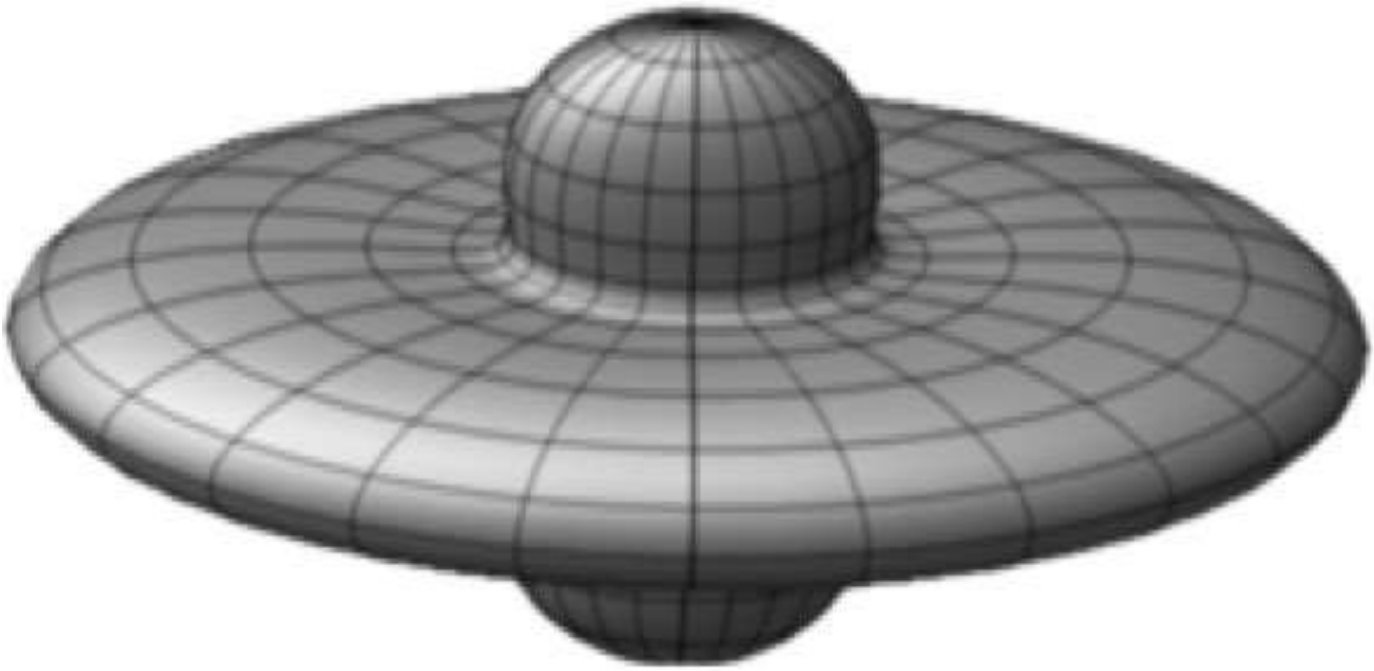

Figure 1. Spherical quatrefoil.

where β_p is the angle between n_p and (Q - P). The formula for the spherical quatrefoil shape is given by (Figure 1):

$$\rho = 0.002 + 0.003 \cos(2\theta)^2$$
$$x = 0.95\rho \sin\theta \cos\phi, \quad 0 < \theta < \pi$$
$$y = 2.07\rho \sin\theta \sin\phi, \quad 0 < \phi < 2\pi$$
$$z = 0.99\rho \sin\theta \cos\phi, \quad 0 \leq \cos 2\theta \leq 1 \qquad (2)$$

The radiosity model generally describes the energy both emitted from and reflected by a surface. The amount of energy that can be emitted from a surface depends only on the temperature of the surface (the Stefan-Boltzmann Law and the Wien's Law) and the emissivity of the material. The energy that strikes the surface is reflected from the surrounding environment.

The illumination at a given point in the environment is a combination of the light emitted by a light source, and the light reflected from the surfaces. We researched the feasibility of obtaining good convergence results for the spherical quatrefoil when the light source is the sun and when there is artificial light located on the exterior of the space but still on the spacecraft; these are named Case I and Case 2.

It is our view that smaller reflectivity values would reduce computational costs associated with obtaining Galerkin coefficients. Compared with earth, Mars has lower surface temperatures, much lower atmospheric absorption and radiation, and higher surface emissivity (Ho et al., 2012). We made the assumption that in Case 1 the light source for the interior Quatrefoil space of the spacecraft originated from outside of the spacecraft thus from the Martian atmosphere (Wheelwright and Toole, 1992). Mars has a large surface emissivity due to the land surfaces having lower dielectric constants. No liquid water surface has been detected on Mars. The soil's moisture and surface roughness affect emissivity, and the color of materials also affects the reflectivity. On the average, earth has lower values of emissivity and reflectivity. Mars has higher average surface emissivity due to the roughness of soil and rocks on the surface. For any surface to maintain a constant temperature, the incoming energy has to be the sum of the energy emitted and reflected. We used the Green's theorem to solve the integral equation on the boundary of the surface for the Dirichlet problem. Previously, multiple surfaces were used to test this method for the Dirichlet condition, such as the spherical rhombus (Warnapala and Deng, 2016). The shapes we are working on is a more realistic shape that is simply connected and bounded and is suitable for the brightness that exits on planet Mars.

The exterior boundary problem for all these surfaces will be solved using the Gaussian quadrature method, where rotations of the coordinates would be used to minimize the inherent singularity that is present in the fundamental solution of the radiosity equation. The boundary condition will only take into account the absorption of the incoming light waves (Atkinson and Chien, 2006). The assumption on the surfaces is that they are Lambertian diffuse reflectors. Brightness of these surfaces are the same regardless of the observer's angle of view, thus they obey the Lambert's Cosine Law or are isotopic.

METHODOLOGY

Fortran 77 software was used for all calculations.

Radiosity model

S is a closed bounded surface in $\Re^3$ and it belongs to the C^2 class. D_+ denotes the exterior of the spherical quatrefoil. Then the radiosity (brightness) equation from computer graphics is given by:

$$u(P) - \frac{\rho(P)}{\pi}\int_S u(Q)G(P,Q)V(P,Q)dS_Q = E(P), P \in S \quad (3)$$

with *E* a given emissivity function. *E* is *I* times continuously differentiable and the I^{th} order derivatives of the surface representations are also Holder continuous with exponent λ. The function spaces we are working with are $L^2(S)$ and $C(S)$ that is, the square-integrable Lebesgue measurable functions and the continuous functions on *S*, respectively.

Formulation of the radiosity integral

The boundary value problem was reformulated as an integral equation. The integral is only solved on the boundary of the spherical quatrefoil.

$$u(P) - \int_S u(Q)\frac{\partial(G(P,Q))}{\partial v_Q} d\sigma_Q \text{ with} P \notin D_+ \quad (4)$$
$$\text{where } r = |P - Q|.$$

where

$$r = |P - Q|$$

This is a weakly singular integral; these types of equations arise in many applications such as in radiation equilibrium applications, electrostatics and potential theory (Colton and Kress, 2013). The kernel $G(P,Q)$ is given by:

$$G(P,Q) = \frac{[(Q-P)\cdot n_P][(P-Q)\cdot n_Q]}{|P-Q|^4}. \quad (5)$$

where n_P is the inner unit normal to S at P, and $V(P,Q) = 1$ (assuming that the points P and Q are in a straight line and does not intersect with the surface at any other point), unclouded surface; Y_n^m, $n = -m,...m$ denote the basis functions that are the linearly independent spherical harmonics of order m given by:

$$Y_n^m(\phi,\theta) = \left(\frac{1}{2\pi}(m+\frac{1}{2})\frac{(m-n)!}{(m+n)!}\right)^{\frac{1}{2}} p_n^m(\cos\theta)e^{im\phi}.$$

$$u(P) - \int_S u(Q)\frac{\partial G(P,Q)}{\partial v_Q} d\sigma_Q = E(P), \quad P \in S \quad (6)$$

The integral equation is given by:

$$u - Ku = E,$$

where $Ku(P) = \int_S u(Q)\frac{\partial}{\partial vQ}\left(\frac{[(Q-P).n_P][(P-Q).n_Q]}{\pi|P-Q|^4}\right)d\sigma_Q \quad (7)$

By the assumptions on $G(P,Q)$, the kernel $\frac{\partial\Psi(P,Q)}{\partial v_Q}$ is bounded on $S \times S$, and is compact from $C(S)$ to $C(S)$ and $L^2(S)$ to $L^2(S)$ (Warnapala and Deng, 2016).

The Galerkin method

The variable of integration in (7) was converted to a new integral equation defined on the unit sphere *U.* The Galerkin method was applied to this new equation, using spherical polynomials to define the approximating subspaces (El-Ajou et al., 2015).

$$m : U \to^{1-1}_{onto} S,$$

where *m* is at least differentiable, for which the following properties are satisfied.

$$E \in C^{l,\lambda}(S) \text{ and } S \in C^{l+1,\lambda} (S \in C^2 \text{ for } l = 0) \text{ implies } \hat{E} \in C^{\iota,\lambda}(U), \quad (8)$$

$$\hat{E}(Q) = E\big(m(Q)\big), Q \epsilon U. \quad (9)$$

By changing the variable of integration in (7) we obtained the new equation over *U* thus:

$$(I-K)\hat{u} = \hat{E}, \hat{E} \epsilon C(U) \quad (10)$$

where $K(P,Q) = \frac{\rho(p)}{\pi}G(P,Q)V(P,Q)$.

The notation ^ denotes the change in variable from *S* to *Unit Sphere*, as in (9). The operator $(I-K)^{-1}$ exists and is bounded on $C(U)$ and $L^2(U)$ (Arqub et al., 2017). The dimension for the approximating subspace of spherical polynomials of degree $\leq N$ is $d = (N+1)^2$: and $\{h_1,...h_d\}$ denotes the basis of spherical harmonics for the Galerkin's method to solve (10) given by:

$$\big(I - P_N\hat{K}\big)\widehat{u_N} = P_N\hat{E} \quad (11)$$

After one computes the Galerkin coefficients α_i by (12), we substitute the coefficients to (13) to find the approximate solution for our problem.

$$\alpha_i\big(h_i,h_i\big) - \sum_{j=1}^d \alpha_j\big(\hat{K}h_j,h_i\big) = \big(\hat{E},h_i\big) i = 1,..d. \quad (12)$$

The numerical solution is thus given by

$$\widehat{u_N} = \sum_{j=1}^d \alpha_j h_j. \quad (13)$$

The convergence of u_N to u in $L^2(S)$ is straightforward in Lin (1982).

Volume and the surface area for the spherical quatrefoil

The quantity of the space enclosed by the shape or volume, was solved by deriving an integral using the spherical quatrefoil's parametric equations and spherical coordinates. The equations of the shape are given by (1). Since $0 < |\cos 2\theta| \leq 1$ and the radius $\rho = |0.002 + 0.003\cos 2\theta| \leq 1$, then it follows that $0.002 \leq \rho \leq 0.005$.

The equation for outer edge of a sphere was derived using the shape's radius and $f(\rho,\theta,\phi) = \sqrt{x^2+y^2+z^2}$. The triple integral we used for the volume is given by:

$$V = \int_0^{2\pi} \int_0^{\pi} \int_{0.002}^{0.005} f(\rho, \theta, \phi) \rho^2 \sin\theta \, d\rho \, d\theta \, d\phi \quad (14)$$

The triple integral includes ranges in all three directions (ρ, θ, ϕ) and was calculated using Python programming language; the approximate value was $2.1628634577527747 \; x \; 10^{-9}$.

The surface area of the spherical quatrefoil is smooth and irregular, but can be approximated using oblate and prolate spheroid surface area formulas as a surface revolution about the z-axis. The general ellipsoid is a quadratic surface where the semi-axes are lengths a, b, and c.

Equal semi-axes lengths assume a spheroid and varying lengths determine oblate or prolate classification. An oblate spheroid is formed by revolving an ellipse about the minor axis:

$$S_{\text{oblate}} = 2\pi a^2 \left(1 + \frac{1-e^2}{e} \tanh^{-1} e\right)$$

where $e^2 = 1 - \frac{c^2}{a^2}$.

Whereas a prolate spheroid is formed by revolving an ellipse about the major axis:

$$S_{\text{prolate}} = 2\pi a^2 \left(1 + \frac{c}{ae} \sin^{-1} e\right)$$

where $e^2 = 1 - \frac{a^2}{c^2}$ (Voigt et al., 2004).

For the horizontal spherical body component of the spherical quatrefoil, ellipticity of the oblate spheroid was used to approximate its surface area. Likewise, the surface area of the vertical spherical body component was approximated using the ellipticity of a prolate spheroid; the approximated value was $3.459603087 \times 10^{-9}$.

Both surface area and volume approximations were calculated for the general (1:1:1) spherical quatrefoil for Case 1. Varying coefficient ratios altered surface area and volume approximations.

Emissivity and reflectivity on Planet Mars

Compared with Earth, Mars has lower surface temperatures and much lower atmospheric absorption and radiation in addition to higher surface emissivity (deGroh et al., 2008). The atmospheric emission from oxygen and water vapor is almost negligible due to very low atmospheric density and optical depth. Martian surface emissivity is closely related to physical temperature and materials on it. Mars has a large surface emissivity due to its land surfaces having lower dielectric constants. No water surface has been detected on Mars. The soil's moisture and surface roughness also affect emissivity. Lower material densities have lower reflectivity. In all, on the average, Earth has lower value of emissivity and reflectivity. However, rocks on Mars usually have lower emissivity.

Surface emissivity (*E*) is related to reflectivity; $E = 1 - \rho$, which means the sum of emissivity and reflectivity is 1. To the naked eye, Mars' has a reddish appearance due to the presence of iron oxide dust (Markiewicz et al., 1999). When light radiates from the sun and shines onto Mars, the sky would appear as orange. Thus, the wavelength and frequency values will be derived from the orange visible light on the electromagnetic spectrum. In using the wavelength of orange visible light as the input of both the functions, it is necessary to obtain an optimal range of varying amplitude. The amplitude of a light wave is important in understanding the brightness or intensity of the light as it measures the amount of energy carried. Since there have not yet been specific amplitude values reported from planet Mars, ranges will be obtained according to convergence results with the smallest absolute error for the sine and its co-function.

NUMERICAL RESULTS

Case 1: Brightness from external light source

Case 1 modeled the potential of harnessing natural lighting from the sun while the spherical quatrefoil is inhabited and stationed on planet Mars. For testing this case, a sine function was used to model the activity and interactions between light components such as wavelength (λ), frequency (v), angular frequency (ω), wave number (k), time in seconds (t), and amplitude (A).

The true solutions tested are given by:

U1 = 3.05 COS (2.18E10-15X + 3.92E10-6Y)

U2 = 0.0003 SIN (2.18E10-15X + 3.92E10-6Y)

U3 = 1 SIN (1.58E-15X - 4.72E10-21Y)

U4 = 2 SIN (1.58E-15X - 4.72E10-21Y)

U5 = 5 SIN (1.58E-15X - 4.72E10-21Y)

U6 = 10 SIN (1.58E-15X - 4.72E10-21Y)

Here the assumption is that the true function and the emissivity are the same. *NINTI* = 32 are the interior nodes used for calculating $\widehat{K}h_j$, *NINTE* = 20 are the exterior nodes used for calculating $(\widehat{K}h_j, h_i)$. *NDEG* = 5 is the degree of the approximate spherical harmonics.

Figure 3a and b are plotted equidistant from the spherical quatrefoil. The graphs show that the amplitude (energy level) of the emissivity function has a small effect on convergence results. The direction of sunlight that gives the brightness of the quatrefoil space has also a small impact on the convergence.

Case 2: Brightness from an internal light source

Research has reported that blue light has strong impacts on dinoflagellates and can be greatly efficient in maintaining synchronized circadian rhythms (Holzman, 2010). Case 2 modeled the illumination inside the spacecraft just outside of the spherical quatrefoil with an internal artificial light source of blue light (Figure 2).

Figure 4 shows that there is much greater accuracy for the points away from the boundary than for points near the boundary, because the integrand is more singular at points near the boundary as the kernel function involves $1/r^2$ which is much more oscillatory. When *r* becomes large, we had to increase the integration nodes to achieve the same accuracy. Also we chose *NINTE* < *NINITI*, because the integrand of $(h_i, \widehat{K}h_j)$ is smoother than the integrand of $\widehat{K}h_j$.

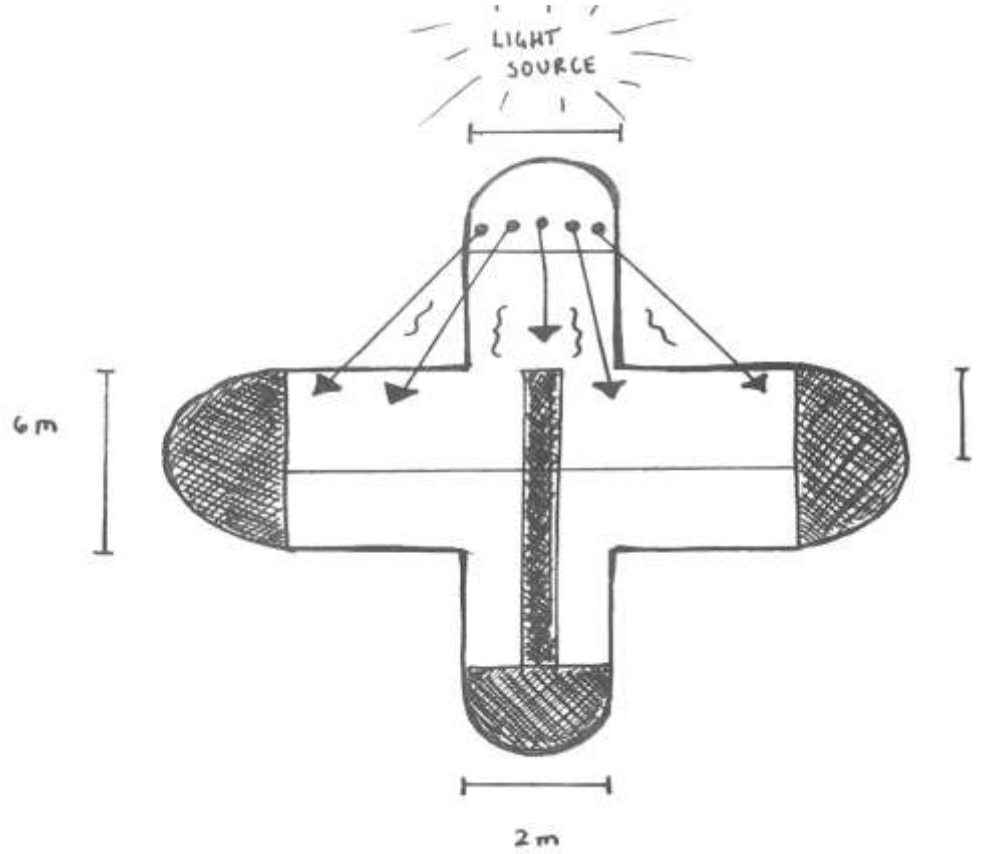

Figure 2. Preliminary sketch of the spherical quatrefoil and its interior configuration.

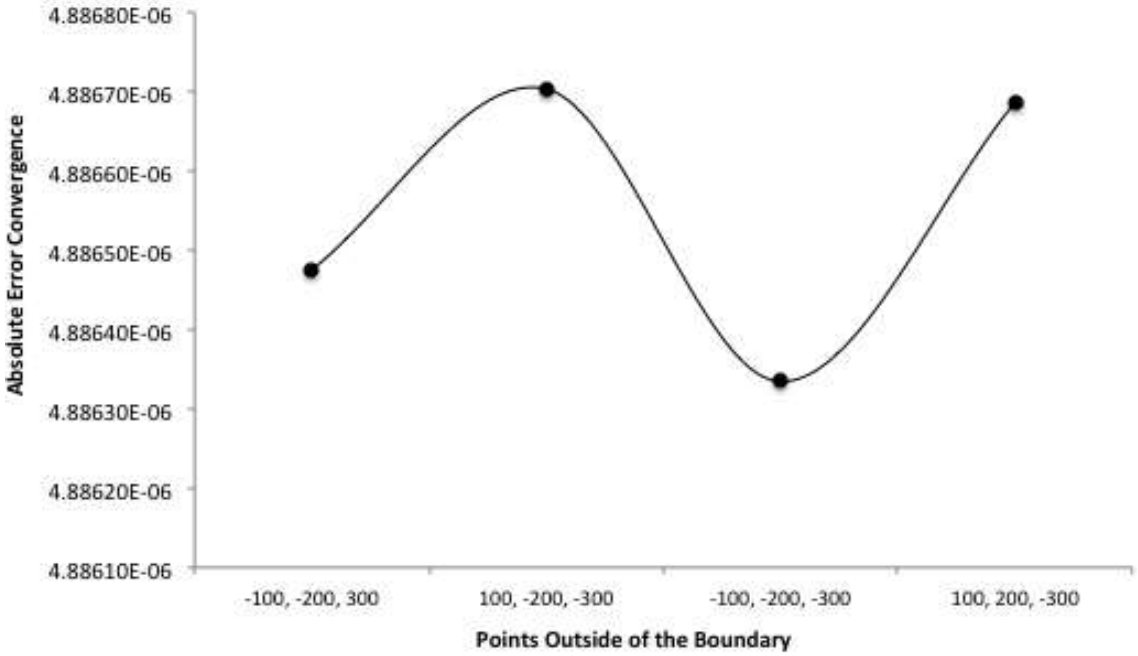

Figure 3a. Convergence results for different points for the true function of U1 = 3.05 COS (2.18E10-15X + 3.92E10-6Y). The wave number was 2.18E10-15, the angular frequency was 3.92E10-6, ρ=0.10, NDEG=5, NINTI=32, NINTE=20, and a coefficient ratio of 1:2:1 for the spherical quatrefoil was used.

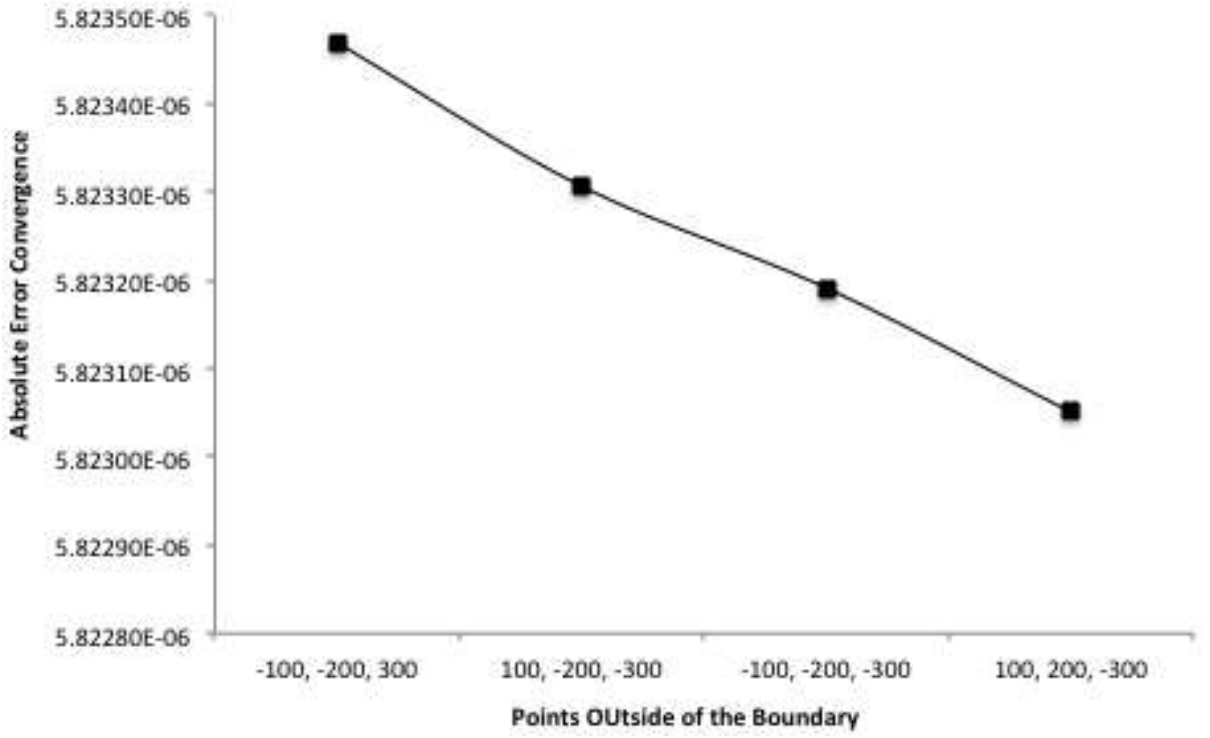

Figure 3b. Convergence results for various points and the true function of U2 = 0.0003 SIN (2.18E10-15X + 3.92E10-6Y). The wave number was 2.18E10-15, the angular frequency was 3.92E10-6, ρ=0.10, NDEG=5, NINTI=32, NINTE=20, and a coefficient ratio of 1:2:1 for the spherical quatrefoil was used.

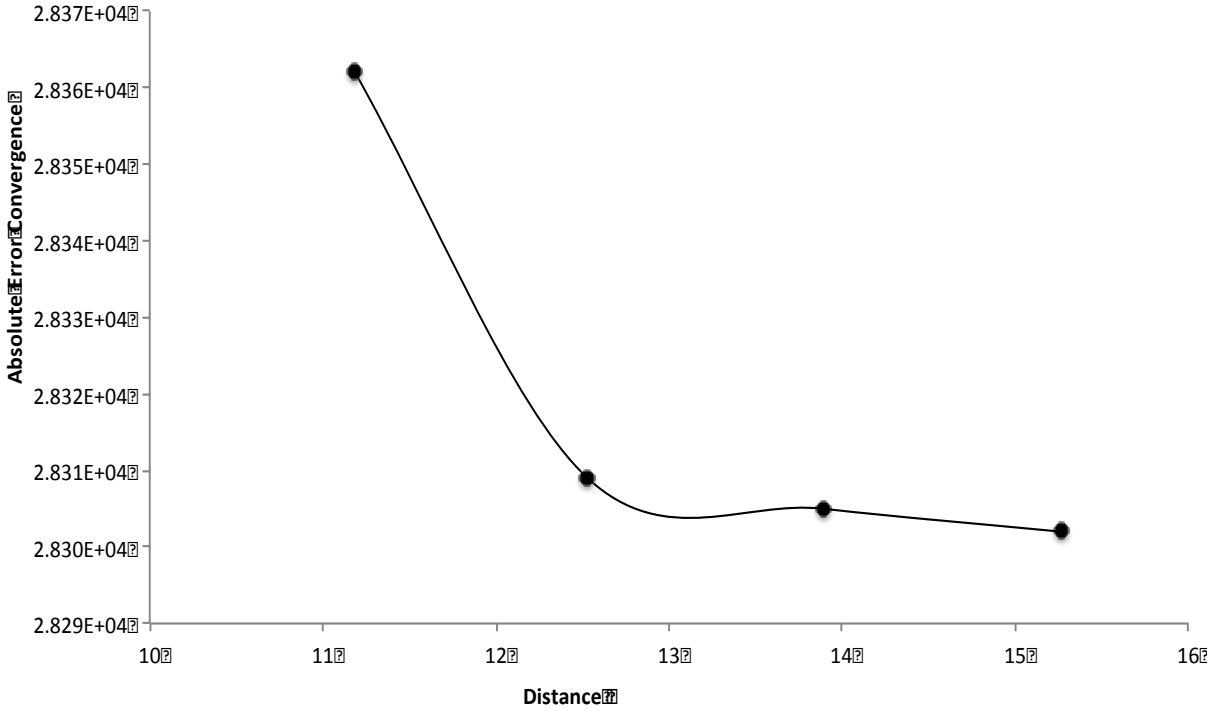

Figure 4. Optimal convergence results for blue light emissivity function of a sine function for various points using an amplitude of 10; emissivity given by U6=10SIN(1.58E-15X-4.72E10-21Y), ρ=0.004, and a coefficient ratio of 1:2:1 for the spherical quatrefoil was used. NDEG=5, NINTI=32, and NINTE=20. Four different points with increasing distance from the boundary of the shape were used.

Table 1. Convergence results for blue emissivity sine function. Emissivity was given by U=A SIN (1.58E-15 X-4.72E10-21 Y). A coefficient ratio of 1:2:1 for the Spherical Quatrefoil and ρ=0.004 was used. NDEG=5, NINTI=32, and NINTE=20. From 4 different directions, 4 different amplitudes (1,2,5 and 10) were used.

Amplitude (A)	Points (x,y,z)	Distance	Absolute Error
1	0,5,10	11.18034	9.3177830568D-06
	0,6,11	12.529964	9.3177830515D-06
	0,7,12	13.892444	9.3177830511D-06
	0,8,13	15.264338	9.3177830508D-06
2	0,5,10	11.18034	9.3177830323D-06
	0,6,11	12.529964	9.3177830270D-06
	0,7,12	13.892444	9.3177830266D-06
	0,8,13	15.264338	9.3177830263D-06
5	0,5,10	11.18034	9.3177829588D-06
	0,6,11	12.529964	9.3177829535D-06
	0,7,12	13.892444	9.3177829530D-06
	0,8,13	15.264338	9.3177829527D-06
10	0,5,10	11.18034	9.3177828362D-06
	0,6,11	12.529964	9.3177828309D-06
	0,7,12	13.892444	9.3177828305D-06
	0,8,13	15.264338	9.3177828302D-06

Conclusion

We conclude that the error is affected by the boundary *S*, boundary data, emissivity, reflectivity and the position of the light source (Table 1). In this case, we found the optimal solution for the number of integration nodes that were used for calculating Galerkin coefficients $(\hat{K}h_j, h_i)$. Aside from investigating the interactions of different metal alloys and various coatings with incoming light waves, future work will also aim to resolve other boundary conditions for the spherical quatrefoil, besides the Dirichlet condition. For instance, there is the Neumann and Robin boundary conditions (Arqub, 2017). Solutions to the radiosity equation are relevant to agencies such as NASA (National Aeronautics and Space Administration) because of their use in energy balancing relationships in isothermal and non-isothermal surfaces and space. The radiosity equation is generally an energy-balanced equation for discrete surfaces (Atkinson, 1982). Since the quality and intensity of brightness depends on the material properties of the surfaces such as color, reflectance and texture, we need to further research on what materials are best to build an interior space to satisfy these requirements. The current emissivity functions used to test the shapes were based on the sine wave function and the cosine function. Our results thus provide a window to an applicable design for an interior space shaped as a spherical quatrefoil with adequate brightness on a spacecraft that might, someday, land on Mars.

CONFLICT OF INTERESTS

The authors have not declared any conflict of interests.

REFERENCES

Arqub OA (2017). Numerical solutions for the Robin time-fractional partial differential equations of heat and fluid flows based on the reproducing kernel algorithm. Int. J. Numer. Methods for Heat Fluid Flow. doi:10.1108/HFF-07-2016-0278.

Arvo J (1995). The Role of the Functional Analysis in Global Illumination, Rendering Techniques '95, edited by PM Hanrahan and W Purgathofer, Springer-Verlag, NY. pp. 115-126.

Atkinson KE (1982). The numerical solution of the Laplace's equation in three dimensions. SIAM J. Numer. Anal. 19:263-274.

Atkinson KE, Chien D (2006). A Study of the Fast Solution of the Occluded Radiosity Equation. Electronic Trans. Numer. Anal. 23:219-250.

Beyer WH (1987). CRC Standard Mathematical Tables, 28th ed. Boca Raton, FL: CRC Press.

Colton D, Kress R (2013). Integral equation methods in scattering theory. Soc. Ind. Appl. Math. pp. 66-90.

DeGroh KK, Banks BA, Dever JA, Jaworske DA, Miller SK, Sechkar EA, Panko SR (2008). NASA Glenn research center's materials international space station experiments (MISSE 1-7). In Proceedings of the International Symposium on "SM/MPAC&SEED" Experiment pp. 91-119.

El-Ajou A, Abu AO, Momani S, Baleanu D, Alsaedi A (2015). A novel expansion iterative method for solving linear partial differential equations of fractional order. Appl. Math. Comput. 257:119-133.

Ho C, Slobin S, Sue M, Njoku E (2012). Mars Background Noise Temperatures. IPN Progress Report. 42-149.

Holzman, DC (2010). What's in a color? The unique human health effects of blue light. Environ. Health Perspect. 118(1):A22-A27.

Lin TC (1982). The numerical solution of the Helmholtz equation using integral equations, Ph.D. thesis, University of Iowa, Iowa City, Iowa.
Markiewicz WJ, Sablotny RM, Keller HU (1999). Optical properties of the Martian aerosols as derived from Imager for Mars Pathfinder midday sky brightness data. J. Geophys. Res. Planets 104(E4):9009-9017.
Voigt A, Hanssen N, Weichmann C (2004). The radiosity equation for solving global heat transfer in industrial furnaces. Math. Comput. Model. 39(2-3):145-150.
Warnapala Y, Deng Q (1982). Numerical solutions of the radiosity's equation for low reflectivity and emissivity on planet Mars. Int. J. Math. Trends Technol. 34:9-14.
Wheelwright CD, Toole JR (1992). Spacecraft lighting systems. Industry Applications Society Annual Meeting, Conference Record of the IEEE. pp. 1840-1845.